

Chiral Induced Spin Selectivity as a Spontaneous Intertwined Order

Xiaopeng Li,^{1,2,*} Jue Nan,³ and Xiangcheng Pan⁴

¹State Key Laboratory of Surface Physics, Institute of Nanoelectronics and Quantum Computing, and Department of Physics, Fudan University, Shanghai 200438, China

²Shanghai Qi Zhi Institute, AI Tower, Xuhui District, Shanghai 200232, China

³State Key Laboratory of Surface Physics, Institute of Nanoelectronics and Quantum Computing, and Department of Physics, Fudan University, Shanghai 200433, China

⁴State Key Laboratory of Molecular Engineering of Polymers, Department of Macromolecular Science, Fudan University, Shanghai 200438, China

(Dated: January 1, 2021)

Chiral induced spin selectivity (CISS) describes efficient spin filtering by chiral molecules. This phenomenon has led to nanoscale manipulation of quantum spins with promising applications to spintronics and quantum computing, since its discovery nearly two decades ago. However, its underlying mechanism still remains mysterious for the required spin-orbit interaction (SOI) strength is unexpectedly large. Here we report a multi-orbital theory for CISS, where an effective SOI emerges from spontaneous formation of electron-hole pairing caused by many-body correlation. This mechanism produces a strong SOI reaching the energy scale of room temperature, which could support the large spin polarization observed in CISS. One central ingredient of our theory is the Wannier functions of the valence and conduction bands correspond respectively to one- and two-dimensional representation of the spatial rotation symmetry around the molecule elongation direction. The induced SOI strength is found to decrease when the band gap increases. Our theory may provide important guidance for searching other molecules with CISS effects.

Introduction.— Atomic spin-orbit coupling is a relativistic quantum effect that originates from the fundamental quantum electrodynamics of electrons orbiting around the nucleus. It is established that heavier atoms tend to have stronger spin-orbit couplings as the effective coupling strength increases with the atomic number Z as Z^4 [1, 2]. Consequently, material research aiming for strong spin-orbit effects has been mainly focusing on materials composed of heavy atoms [2].

However, a surprisingly large spin-orbit effect has been found in chiral organic and biological molecules mainly composed of carbon atoms in the study of chiral induced spin selectivity [3], which has received enormous research efforts in the last decade [4–18]. This fascinating phenomenon has been observed in a broad range of chiral molecules, from DNA [3, 6] and protein [8], to α -helical peptides [11, 14] and helicene [12, 16], using a number of different experimental setups such as photoelectron transmission [3, 6], transport [7, 12, 14], and electrochemistry measurements [19]. It has far reaching implications in the fundamental understanding of important biological processes such as protein-folding and biorecognition [4]. The experimental observations imply a generic underlying mechanism of spin filtering by chiral molecules, that demands a theoretical explanation. Previous theoretical studies have shown that a sufficiently strong SOI is required for tight-binding models to reproduce the experimental features [20–23], although the intrinsic spin orbit interaction in these molecules mainly containing carbon atoms is too weak to accommodate

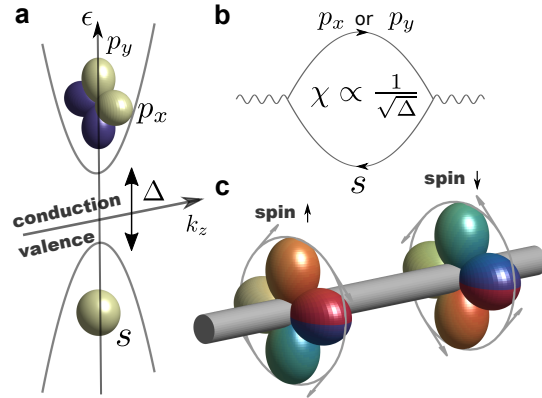


FIG. 1. **Electron-hole pairing in the three-orbital model.** **a**, Illustration of the three orbital (s , p_x , and p_y) model. The valence and conduction bands have s - and p -orbital character, respectively. The band gap is Δ . **b**, The Feynman diagram that leads to the divergent susceptibility towards forming electron-hole pairing across the valence and conduction bands. **c**, Sketch of the spin-orbit intertwined order with the spin and angular-momentum of the electron-hole pair spontaneously coupled.

the observed large spin polarization, for example up to 60% using chiral peptide molecules [14]. The essential question that remains outstanding is how the unexpectedly strong SOI emerges [24] beyond the conventional consideration of the quantum electrodynamics.

In the study of atomic Bose-Einstein condensates,

a quantum fluctuation enabled spin-momentum intertwined order has been proposed in theory [25] to explain the observed spin-momentum locking in a hexagonal optical lattice without bare SOI [26]. This mechanism has been further generalized to a multi-orbital Bose-Einstein condensate, where a spontaneous spin angular-momentum intertwined order is shown to occur in a metastable state for spinor Bosons residing on excited bands of a square lattice [27]. These theoretical studies are inspiring, suggesting that spin-orbit coupling could emerge from many-body correlation even in complete absence of single-particle SOI, although the bosonic theories do not apply to electrons bearing CISS in chiral molecules.

In this work, we assume a rotation symmetry around the molecule elongation direction (to be referred as z below), and consider a setup where electronic valence and conduction bands correspond to a one- and two-dimensional representation of the symmetry group, respectively. The Wannier functions then have s and p -orbital character (Fig. 1). Through field theory analysis and renormalization group calculation, we show the electron correlation causes a strong instability towards forming electron-hole pairs that spontaneously break the spin SU(2) and reflection symmetries with preservation of time-reversal. This spontaneous spin-orbit intertwined order gives rise to a strong SOI having a first-quantization form

$$\lambda_{\text{so}} \hat{\sigma}_z \otimes \hat{L}_z / 2, \quad (1)$$

with $\hat{\sigma}_z$ the spin Pauli- z operator and \hat{L}_z the angular momentum operator for p -orbitals in the conduction band. Considering a band gap Δ , s - and p -orbital tunnelings, t_s and t_p , and their interactions including density-density interaction U , Hund's rule coupling J , and Josephson coupling J' [28], the induced SOI strength is given as

$$\lambda_{\text{so}} = \Delta/2 - \sqrt{\Delta^2/4 + (U - J - J')^2 |\phi|^2} / 2, \quad (2)$$

with $|\phi|$ the amplitude of the spin-orbit intertwined order parameter estimated to be $|\phi| = 0.25 \times (U - J - J') / (t_s + t_p)$ in the small band gap limit. Taking an example of $t_s + t_p = 2$ eV, $U - J - J' = 1$ eV and $\Delta = 0$ —the parameter choice corresponds to an interaction estimate [28] for a right-handed peptide 3_{10} helix with a triplet-paired band structure [29]—the induced SOI reaches 0.1 eV, which suffices for modeling the unexpectedly large CISS effects in chiral molecules that persist upto room temperature [24]. The strength of the induced SOI decreases when the band gap is increased. We expect this result would strongly contribute to the understanding of spin-selective processes in biology [4].

Our theory starts from a field theory description of the three-orbital system (Fig. 1),

$$\hat{H}_0 = \int dz \sum_{\nu, \alpha} P_\nu \hat{\Psi}_{\nu\alpha}^\dagger(z) \left[\frac{\hbar^2 \partial_z^2}{2m_\nu} - \frac{\Delta}{2} \right] \hat{\Psi}_{\nu\alpha}(z). \quad (3)$$

Here $\nu = s, p_x,$ or p_y index the orbitals, and α the spin degrees of freedom; P_ν represents the parity, i.e., $+$ and $-$ for s - and p -orbitals, respectively; m_s and $m_{p_x} = m_{p_y} \equiv m_p$ the effective mass associated with the motional dynamics of the valence and conduction bands along the molecular elongation direction. The field operators $\hat{\Psi}_{\nu\sigma}$ incorporates the low energy degrees of freedom of electrons moving in a molecule near the band edge. For example, in modeling a right-handed peptide helix with a triplet-paired band structure [29], our three-orbital model corresponds to an effective description of electronic properties of the molecule, with s and p -orbitals representing the quantized transverse modes. Considering a carbon atomic chain, our theory corresponds to the Fermi energy lying in between the sp -hybridized σ^* -bond and π -bond. We remark that the s -orbital in our model may represent a p_z orbital in the molecule as well, which obeys the same symmetry under the spatial rotation around the z direction.

An immediate consequence of the field theory is that it develops strong susceptibility towards electron-hole pairing at low temperature even without interaction. This is described by a response function, $\chi_{sp}^0 = \partial_h \langle \hat{\Psi}_{s\alpha}^\dagger \hat{\Psi}_{p\alpha'} + H.c. \rangle = \sqrt{(m_s^{-1} + m_p^{-1})} / 2\Delta$, considering a fictitious infinitesimal perturbation $\Delta H = -h \int dz \left[\hat{\Psi}_{s\alpha}^\dagger \hat{\Psi}_{p\alpha'} + H.c. \right]$. This response has a divergent behavior $1/\sqrt{\Delta}$ for a small band gap, which is caused by the interplay of the logarithmic divergence of the Feynman diagram (Fig. 1) and the van Hove singularity in one dimensional density of states. In order to have spin-orbit coupled effect from the divergent electron-hole pairing, the idea here is to form a quantum superposition between the s -orbital and the finite angular momentum $p_x \pm ip_y$ state that preserves time-reversal symmetry. This would then provide the required effective spin-orbit coupling. To form an orbital superposition in this channel, we need to assume that the Wannier functions of the valence and conduction bands correspond respectively to one- and two-dimensional representation of the spatial rotation symmetry around the molecule elongation direction. Such physics does not occur in the previous study of correlation effects in a single-band setting [23].

The divergence in the response function indicates important many-body effects in the system. Having spin SU(2) and spatial rotation symmetries, the three in-

j_s, m_s, m_l	Operators	SU(2)	Parity	TRS
0, 0, 0	$\hat{\mathcal{B}}_{0,0,0;0}, (\hat{\mathcal{B}}_{0,0,0;+1} + \hat{\mathcal{B}}_{0,0,0;-1})/\sqrt{2}$ $(\hat{\mathcal{B}}_{0,0,0;+1} - \hat{\mathcal{B}}_{0,0,0;-1})/\sqrt{2}$	Singlet	Even	Even Odd
0, 0, 1	$(\hat{\mathcal{B}}_{0,0,1;0} + \hat{\mathcal{B}}_{0,0,1;-1})/\sqrt{2}$ $(\hat{\mathcal{B}}_{0,0,1;0} - \hat{\mathcal{B}}_{0,0,1;-1})/\sqrt{2}$	Singlet	Odd	Even Odd
0, 0, 2	$\hat{\mathcal{B}}_{0,0,2;-1}$	Singlet	Even	Even
$1, m_s \in \{0, \pm 1\}, 0$	$\hat{\mathcal{B}}_{1,m_s,0;0}, (\hat{\mathcal{B}}_{1,m_s,0;+1} + \hat{\mathcal{B}}_{1,m_s,0;-1})/\sqrt{2}$ $(\hat{\mathcal{B}}_{1,m_s,0;+1} - \hat{\mathcal{B}}_{1,m_s,0;-1})/\sqrt{2}$	Triplet	Even	Odd Even
$1, m_s \in \{0, \pm 1\}, 1$	$(\hat{\mathcal{B}}_{1,m_s,1;0} + \hat{\mathcal{B}}_{1,m_s,1;-1})/\sqrt{2}$ $(\hat{\mathcal{B}}_{1,m_s,1;0} - \hat{\mathcal{B}}_{1,m_s,1;-1})/\sqrt{2}$	Triplet	Odd	Odd Even
$1, m_s \in \{0, \pm 1\}, 2$	$\hat{\mathcal{B}}_{1,m_s,2;-1}$	Triplet	Even	Odd

TABLE I. **Symmetry properties of electron-hole pairings.** We have introduced quantum numbers j_s and m_s according to the spin SU(2) symmetry, with j_s equal to 0 and 1 labeling singlet and triplets. Under a spatial rotation around the z direction by an angle θ , the operators transform as $B_{j_s, m_s, m_l; q} \rightarrow B_{j_s, m_s, m_l; q} e^{im_l \theta}$, determined by the quantum number m_l . Under time-reversal symmetry (TRS) transformation, we have $B_{j_s, m_s, m_l; q} \rightarrow (-)^{j_s+1} (-)^{m_l+m_s} B_{j_s, -m_s, -m_l; -q}$. The even/odd sign of TRS listed here is determined for an operator $\hat{\mathcal{O}}$ according to whether its corresponding Hermitian observable $h\hat{\mathcal{O}} + h^* \hat{\mathcal{O}}^\dagger$ (with h an arbitrary complex number) is TRS even or odd. The operators with $m_l = 0, -1, -2$ are not listed here due to the constraint that $B_{j_s, m_s, m_l; q}^\dagger = (-)^{m_l+m_s+1} B_{j_s, -m_s, -m_l; q+m_l}$.

teraction terms including density-density interaction U , Hund's rule coupling J , and Josephson coupling J' [28] are the only allowed local interactions between the s - and p -orbitals. Due to the multi-orbital complexity of our model, there are 21 independent channels in the particle-hole pairing function, $G_{v\alpha, v'\alpha'} = \langle \hat{\psi}_{v\alpha}^\dagger \hat{\psi}_{v'\alpha'} \rangle$. According to symmetry properties, we group all the particle-hole pairings into the following channels,

$$\hat{\mathcal{B}}_{j_s, m_s, m_l; q} = (-1)^{q+1} \sum_{\alpha\alpha'} i^{2\alpha} C_{\frac{1}{2}\frac{1}{2}}(-\alpha, \alpha' | j_s, m_s) \hat{\psi}_{q\alpha}^\dagger \hat{\psi}_{q+m_l\alpha'} \quad (4)$$

where the $C_{\frac{1}{2}\frac{1}{2}}$ matrix contains Clebsch-Gordon coefficients, and $\hat{\psi}_{q\alpha}$ is a field operator in angular momentum basis defined by $[\hat{\psi}_\pm \equiv \mp(\hat{\psi}_x \pm i\hat{\psi}_y)/\sqrt{2}, \hat{\psi}_0 \equiv \hat{\psi}_z]$. The symmetry properties of these operators are listed in Table I.

In order to generate effective SOI with no spin polarization, we shall consider a spin-orbit intertwined order that breaks spin SU(2) symmetry and preserves time reversal symmetry. From Table I, the potential candidates are,

$$\hat{\mathcal{O}}_{m_s} \equiv \frac{1}{\sqrt{2}} [\mathcal{B}_{1, m_s, -1; 0} - \mathcal{B}_{1, m_s, -1; 1}], \quad (5)$$

and

$$\hat{\mathcal{O}}'_{m_s} \equiv \frac{1}{\sqrt{2}} [\mathcal{B}_{1, m_s, 0; 1} - \mathcal{B}_{1, m_s, 0; -1}], \quad (6)$$

whose parities are odd and even, respectively. They both satisfy the symmetry requirement, but the parity even

operators represent parings within s or p -bands, which do not benefit from the divergent susceptibility in our model. We thus focus on analyzing the parity odd spin-orbit intertwined operators $\hat{\mathcal{O}}_{m_s}$. We emphasize here that this symmetry channel would not be possible in a single-orbital model, where a local triplet order necessarily breaks time-reversal symmetry.

Considering a weak Josephson coupling J' , the susceptibility towards forming an order of $\hat{\mathcal{O}}_{m_s}$ is,

$$\chi_{\text{SO}} = \frac{\chi_{sp}^0}{1 - (U - J)\chi_{sp}^0} \quad (7)$$

under random phase approximation [28]. The divergence in the susceptibility for the non-interacting model at zero temperature persists to finite band gap and finite temperature, provided that $U > J$. This requirement is satisfied considering a typical situation for electrons in a molecule, that the density-density interaction is repulsive and the Hund's rule coupling is ferromagnetic ($J < 0$ in our notation). Without Josephson coupling, i.e., $J' = 0$, a degenerate channel— $[\mathcal{B}_{1, m_s, -1; 0} + \mathcal{B}_{1, m_s, -1; 1}]/\sqrt{2}$ which would break time reversal symmetry yields a susceptibility of an identical strength. A negative Josephson coupling $J' < 0$ would break this degeneracy, and make the time reversal symmetric pairing more favorable. In the case of Josephson coupling being negligible, as is expected for elongated chiral molecules (see Supplementary Material), the presence of orbital motion induced Zeeman splitting selects the time reversal symmetric over the asymmetric pairing.

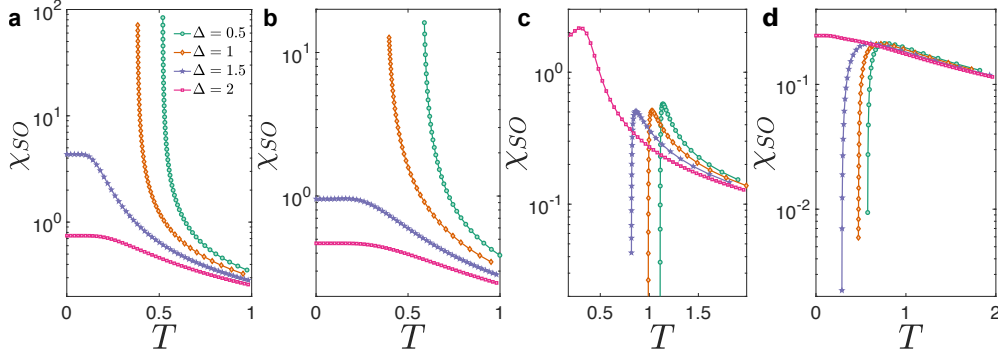


FIG. 2. **Divergent susceptibility for a spin-orbit intertwined order with renormalization group calculation.** The plots correspond to different choices of interaction strengths (U, J, J') and band gap (Δ) in the tight binding model [28]. The tunneling of the p -orbital electron, or one half of bandwidth of the p -band is set as the energy unit here. In (a, b, c, d), we have $(U, J, J') = (2, 0, 0)$, $(U, J, J') = (2, -1, -0.5)$, $(2, 0.1, -0.5)$, and $(2, -1, 0.5)$, respectively, and set the s -band tunneling $t_s = 2$. With both of J and J' negligible (set to zero in this plot) in (a), a divergent susceptibility at finite temperature (T) in the time-reversal symmetric spin-orbit intertwined channel (Eq. (6)) is confirmed, which agrees with the analytical results from random phase approximation. In (b), we find that with both of J and J' being negative, the susceptibility in the spin-orbit intertwined channel is more strengthened, compared to (a). In (c), we find that a positive Hund's rule coupling $J > 0$ does not immediately cause suppression of the spin-orbit intertwined order. (d) shows that a positive Josephson coupling $J' > 0$ does not support the time-reversal symmetric spin-orbit intertwined order.

Since all parity odd pairing channels in our theory potentially have a large susceptibility due to the divergence in χ_{sp}^0 , we further go beyond the random phase approximation, and carry out a systematic summation of Feynman diagrams using a scheme of renormalization group flow equation, which incorporates the intertwined scatterings among different channels [30]. The results for the susceptibility of forming the spin-orbit intertwined order in Eq. 6 are shown in Fig. 2. It is confirmed that having J and J' vanishing, the susceptibility for $\hat{\mathcal{O}}_{m_s}$ diverges at finite temperature (Fig. 2a). The chiral peptide 3_{10} helix corresponds to this case according to interaction strength estimate [28]. The divergence requires the interaction energy to conquer the band gap barrier of the sp -orbital pairing. The susceptibility is more strengthened for both J and J' being negative (Fig. 2b). We also find that having a weak antiferromagnetic coupling in J still supports divergent susceptibility in $\hat{\mathcal{O}}_{m_s}$ channel (Fig. 2c). For a large enough positive J , this susceptibility is no longer divergent, but instead meets a strong suppression at low temperature, which is due to a divergent susceptibility in a different channel, $\hat{\mathcal{B}}_{0,0,\pm 1,q}$ [28]. A sign change in the Josephson coupling leads to a low-temperature suppression of $\hat{\mathcal{O}}_{m_s}$ pairing (Fig. 2 d), owing to a divergent susceptibility in the time-reversal odd channel of $[\mathcal{B}_{1,m_s,-1;0} + \mathcal{B}_{1,m_s,-1;1}]/\sqrt{2}$ [28]. We expect that further considering scattering with additional orbitals present in molecules would renormalize J' to the negative side due to BCS channels [30], which would make

the time-reversal symmetric spin-orbit intertwined order even more favorable.

A divergence in the susceptibility χ_{SO} implies the correlation length of $\langle \hat{\mathcal{O}}_{m_s}^\dagger(z) \hat{\mathcal{O}}_{m_s}(z') \rangle$ reaches the size of the molecule. Taking mean field approximation, the operator $\hat{\mathcal{O}}_{m_s}$ acquires a finite expectation value, $\langle \hat{\mathcal{O}}_{m_s} \rangle \equiv \Phi_{m_s}$. The free energy of the order parameter takes an SU(3) symmetric form as shown in Supplementary Material. The pairings with different m_s quantum numbers $0, \pm 1$ are degenerate, although they lead to two distinctive many-body states, analogous to the spin-1 polar and ferromagnetic superfluids in spinor condensate [31, 32] or liquid Helium [33].

Further considering a circular motion induced Zeeman splitting for electrons [22], we have a perturbative coupling $\Delta H = \delta \int dz [i\psi_{x\uparrow}^\dagger \psi_{y\uparrow} - i\psi_{x\downarrow}^\dagger \psi_{y\downarrow} + H.c.]$. Despite its insufficient strength to model CISS [22, 24], this term determines a spin quantization axis, and triggers an order ($\Phi_{+1} \equiv \phi, \Phi_0 = 0, \Phi_{-1} = 0$) to minimize to total free energy in our theory, from which a strong SOI emerges from electron correlation,

$$H_{SOI} = \frac{U-J-J'}{4\sqrt{2}} \int dz [i\phi \Psi^\dagger(z) \sigma_+ \otimes L_- \Psi(z) + H.c.], \quad (8)$$

with $\Psi \equiv [\psi_{1,\uparrow}, \psi_{0,\uparrow}, \psi_{-1,\uparrow}, \psi_{1,\downarrow}, \psi_{0,\downarrow}, \psi_{-1,\downarrow}]^T$, σ_+ and L_- the standard spin-1/2 and spin-1 angular momentum matrices [28].

This correlation induced coupling breaks spin SU(2) and reflection symmetries with the time reversal sym-

metry unbroken. Through a unitary transformation into the quasi-particle basis, the induced coupling in the conduction band takes a more standard SOI form given in Eq. (2). The induced SOI strength for the quasi-particles reaches to the order of the energy scale of room temperature, and is sufficient to model the spin dependent transmission observed in chiral molecule experiments [24].

We remark here that Mermin-Wegner theorem does not forbid the long-range order formation in our setup as the continuous symmetries of spatial rotation and the spin SU(2) are all weakly broken considering the real geometry of a chiral molecule and the circular motion induced Zeeman splitting.

Discussion.— We have developed a novel quantum mechanism for strong SOI to emerge from many-body correlation effect. This provides an alternative origin for SOI, other than the fundamental quantum electrodynamics, which is particularly crucial to the understanding of the large CISS observed in chiral organic molecules, where the bare SOI is too weak for modeling the experimental observation. Our theory may provide important guidance for future searching of other chiral molecules with CISS, and potentially contributes to the fundamental understanding of spin-selective biological processes.

Since SOI plays an important role in topological physics in general, we expect the mechanism of correlation induced SOI may also shed light on engineering of topological devices such as Majorana quantum computing qubits and also neutral-atom based quantum simulations of topological physics where the bare SOI is absent.

Acknowledgements. We acknowledge helpful discussion with Martin Plenio, Mikhail Lemeshko, Gang Chen, Hongjun Xiang, and Yinghai Wu. This work is supported by National Program on Key Basic Research Project of China (Grant No. 2017YFA0304204), National Natural Science Foundation of China (Grants No. 11934002 and 11774067), Natural Science Foundation of Shanghai City (Grant No. 19ZR1471500), Shanghai Municipal Science and Technology Major Project (Grant No. 2019SHZDZX01).

* xiaopeng_li@fudan.edu.cn

- [1] Herman, F., Kuglin, C. D., Cuff, K. F. & Kortum, R. L. Relativistic corrections to the band structure of tetrahedrally bonded semiconductors. *Phys. Rev. Lett.* **11**, 541–545 (1963).
- [2] Witczak-Krempa, W., Chen, G., Kim, Y. B. & Balents, L. Correlated quantum phenomena in the strong spin-orbit regime. *Annual Review of Condensed Matter Physics* **5**, 57–82 (2014).
- [3] Ray, K., Ananthavel, S., Waldeck, D. & Naaman, R. Asymmetric scattering of polarized electrons by organized organic films of chiral molecules. *Science* **283**, 814–816 (1999).
- [4] Naaman, R., Paltiel, Y. & Waldeck, D. H. Chiral molecules and the electron spin. *Nature Reviews Chemistry* **3**, 250–260 (2019).
- [5] Naaman, R. & Waldeck, D. H. Chiral-induced spin selectivity effect. *The journal of physical chemistry letters* **3**, 2178–2187 (2012).
- [6] Göhler, B. *et al.* Spin selectivity in electron transmission through self-assembled monolayers of double-stranded dna. *Science* **331**, 894–897 (2011).
- [7] Xie, Z. *et al.* Spin specific electron conduction through dna oligomers. *Nano letters* **11**, 4652–4655 (2011).
- [8] Mishra, D. *et al.* Spin-dependent electron transmission through bacteriorhodopsin embedded in purple membrane. *Proceedings of the National Academy of Sciences* **110**, 14872–14876 (2013).
- [9] Dor, O. B., Yochelis, S., Mathew, S. P., Naaman, R. & Paltiel, Y. A chiral-based magnetic memory device without a permanent magnet. *Nature communications* **4**, 1–6 (2013).
- [10] Ben Dor, O., Morali, N., Yochelis, S., Baczewski, L. T. & Paltiel, Y. Local light-induced magnetization using nanodots and chiral molecules. *Nano letters* **14**, 6042–6049 (2014).
- [11] Eckshtain-Levi, M. *et al.* Cold denaturation induces inversion of dipole and spin transfer in chiral peptide monolayers. *Nature communications* **7**, 10744 (2016).
- [12] Kiran, V. *et al.* Helicene, a new class of organic spin filter. *Advanced Materials* **28**, 1957–1962 (2016).
- [13] Dor, O. B. *et al.* Magnetization switching in ferromagnets by adsorbed chiral molecules without current or external magnetic field. *Nature communications* **8**, 1–7 (2017).
- [14] Aragonès, A. C. *et al.* Measuring the spin-polarization power of a single chiral molecule. *Small* **13**, 1602519 (2017).
- [15] Fontanesi, C., Capua, E., Paltiel, Y., Waldeck, D. H. & Naaman, R. Spin-dependent processes measured without a permanent magnet. *Advanced Materials* **30**, 1707390 (2018).
- [16] Kettner, M. *et al.* Chirality-dependent electron spin filtering by molecular monolayers of helicenes. *The journal of physical chemistry letters* **9**, 2025–2030 (2018).
- [17] Smolinsky, E. Z. *et al.* Electric field-controlled magnetization in gaas/algaas heterostructures—chiral organic molecules hybrids. *The journal of physical chemistry letters* **10**, 1139–1145 (2019).
- [18] Koplovitz, G. *et al.* Single domain 10 nm ferromagnetism imprinted on superparamagnetic nanoparticles using chiral molecules. *Small* **15**, 1804557 (2019).
- [19] Mondal, P. C. *et al.* Chiral conductive polymers as spin filters. *Advanced Materials* **27**, 1924–1927 (2015).
- [20] Guo, A.-M. & Sun, Q.-f. Spin-selective transport of electrons in dna double helix. *Physical review letters* **108**, 218102 (2012).
- [21] Gutierrez, R., Díaz, E., Naaman, R. & Cuniberti, G. Spin-selective transport through helical molecular sys-

- tems. *Physical Review B* **85**, 081404 (2012).
- [22] Naaman, R. & Waldeck, D. H. Spintronics and chirality: spin selectivity in electron transport through chiral molecules. *Annual review of physical chemistry* **66**, 263–281 (2015).
- [23] Fransson, J. Chirality-induced spin selectivity: The role of electron correlations. *The Journal of Physical Chemistry Letters* **10**, 7126–7132 (2019).
- [24] Rebergen, M. A study of induced spin selectivity in chiral molecules (2018).
- [25] Li, X., Natu, S. S., Paramakanti, A. & Sarma, S. D. Chiral magnetism and spontaneous spin hall effect of interacting bose superfluids. *Nature communications* **5**, 1–7 (2014).
- [26] Soltan-Panahi, P., Lühmann, D.-S., Struck, J., Windpassinger, P. & Sengstock, K. Quantum phase transition to unconventional multi-orbital superfluidity in optical lattices. *Nature Physics* **8**, 71–75 (2012).
- [27] Li, Y., Yuan, J., Hemmerich, A. & Li, X. Rotation-symmetry-enforced coupling of spin and angular momentum for p-orbital bosons. *Physical review letters* **121**, 093401 (2018).
- [28] See Supplementary Material for description of technical details, which includes Refs. [34, 35].
- [29] Liu, Y., Xiao, J., Koo, J. & Yan, B. Chirality induced topological nature of electrons in dna-like materials (2020). 2008.08881.
- [30] Metzner, W., Salmhofer, M., Honerkamp, C., Meden, V. & Schönhammer, K. Functional renormalization group approach to correlated fermion systems. *Reviews of Modern Physics* **84**, 299 (2012).
- [31] Ohmi, T. & Machida, K. Bose-einstein condensation with internal degrees of freedom in alkali atom gases. *Journal of the Physical Society of Japan* **67**, 1822–1825 (1998).
- [32] Ho, T.-L. Spinor bose condensates in optical traps. *Physical review letters* **81**, 742 (1998).
- [33] Volovik, G. E. *The universe in a helium droplet*, vol. 117 (Oxford University Press on Demand, 2003).
- [34] Weinberg, S. *The quantum theory of fields*, vol. 1: Foundations (1995).
- [35] Marzari, N., Mostofi, A. A., Yates, J. R., Souza, I. & Vanderbilt, D. Maximally localized wannier functions: Theory and applications. *Rev. Mod. Phys.* **84**, 1419–1475 (2012).
-

Supplementary Material

S-1. TIGHT BINDING MODEL

The tight binding Hamiltonian corresponding to the field theory in Eq. (3) is

$$\begin{aligned}
 H_0 = & \frac{\Delta}{2} \sum_{j\alpha} \left[c_{p_x\alpha,j}^\dagger c_{p_x\alpha,j} + c_{p_y\alpha,j}^\dagger c_{p_y\alpha,j} - c_{s\alpha,j}^\dagger c_{s\alpha,j} \right] \\
 & + t_s \sum_{j\alpha} \left[c_{s\alpha,j}^\dagger c_{s\alpha,j+1} + c_{s\alpha,j}^\dagger c_{s\alpha,j-1} - 2c_{s\alpha,j}^\dagger c_{s\alpha,j} \right] \\
 & - t_p \sum_{j\alpha, v=p_x, p_y} \left[c_{v\alpha,j}^\dagger c_{v\alpha,j+1} + c_{v\alpha,j}^\dagger c_{v\alpha,j-1} - 2c_{v\alpha,j}^\dagger c_{v\alpha,j} \right],
 \end{aligned} \tag{S1}$$

with j the site index of the tight binding model, t_s and t_p the nearest neighboring tunneling of the s - and p - orbitals, and $c_{v\alpha}$ the lattice annihilation operator associated with $\psi_{v\alpha}$. The energy dispersion of the tight binding model is $\varepsilon_v(k) = 2t_v(1 - \cos k)P_v$. The tunneling parameters relate to the effective mass in the field theory as $m_v^{-1} = 2t_v/\hbar^2$, taking the lattice constant as a length unit.

Taking spin SU(2) and rotation symmetries, the local electron interaction between s - and p -orbitals involves a density-density term,

$$U \sum_j C_{v,j}^\dagger C_{v,j} C_{s,j}^\dagger C_{s,j} \tag{S2}$$

the Hund's rule coupling,

$$J \sum_{v=p_x, p_y} C_{v,j}^\dagger \vec{\sigma} C_{v,j} \cdot C_{s,j}^\dagger \vec{\sigma} C_{s,j}, \tag{S3}$$

and a Josephson coupling,

$$J' \sum_j \left[\left(c_{p_x\uparrow,j}^\dagger c_{p_x\downarrow,j}^\dagger + c_{p_y\uparrow,j}^\dagger c_{p_y\downarrow,j}^\dagger \right) c_{s\downarrow,j} c_{s\uparrow,j} + H.c. \right], \tag{S4}$$

where we have introduced compact notation, $C_{v,j} \equiv [c_{v,\uparrow,j}, c_{v,\downarrow,j}]^T$. The intra-orbital interaction within the valence band or the conduction band is not included here because only the inter-band interactions contribute strongly to the divergent susceptibility considering the divergence in χ_{sp}^0 .

S-2. RENORMALIZATION GROUP FLOW

In the calculation of susceptibility, we use the scheme of renormalization group flow to carry out a systematic resummation of higher order Feynman diagrams, in order to capture the complex intertwined scatterings among different channels in our theory. Having SU(2) symmetry, the one particle irreducible (1PI) four point function

$$\Gamma_{v_1\alpha_1, v_2\alpha_2; v_3\alpha_3, v_4\alpha_4} = \langle \psi_{v_1\alpha_1} \psi_{v_2\alpha_2} \psi_{v_3\alpha_3}^\dagger \psi_{v_4\alpha_4}^\dagger \rangle_{1PI}, \tag{S5}$$

takes a restricted form

$$\begin{aligned}
 & \Gamma_{v_1\alpha_1, v_2\alpha_2; v_3\alpha_3, v_4\alpha_4} \\
 & = V_{v_1 v_2 v_3 v_4} \delta_{\alpha_1 \alpha_4} \delta_{\alpha_2 \alpha_3} - V_{v_2 v_1 v_3 v_4} \delta_{\alpha_1 \alpha_3} \delta_{\alpha_2 \alpha_4}
 \end{aligned} \tag{S6}$$

This function takes real values according to the time-reversal symmetry. Further considering rotation symmetry, the nonzero ones are $V_{ssss}, V_{xxxx} = V_{yyyy}, V_{ssxx} = V_{ssyy} = V_{xxss} = V_{yyss}, V_{sxxx} = V_{syyy} = V_{xssx} = V_{ysyy}, V_{xssx} = V_{ysyy}, V_{xssx} = V_{ysyy}, V_{xssx} = V_{ysyy}, V_{xssx} = V_{ysyy}, V_{xssx} = V_{ysyy}$,

$V_{xxyy} = V_{yyxx}$, $V_{xyxy} = V_{yxxy}$, $V_{xyyx} = V_{yyxx}$. These four point functions are obtained by solving a renormalization group flow equation [30],

$$\begin{aligned} & \partial_l V(v_1, v_2, v_3, v_4) \\ &= \sum_{v'v''} \left\{ -\dot{\Pi}_{v'v''}^{\text{pp}} V_{v_1 v_2 v'v''} V_{v'v'' v_3 v_4} + 2\dot{\Pi}_{v'v''}^{\text{ph}} V_{v_1 v'v'' v_4} V_{v v_2 v_3 v'} \right. \\ & \quad \left. - \dot{\Pi}_{v'v''}^{\text{ph}} [V_{v_1 v v_3 v'} V_{v'v_2 v v_4} + V_{v v_2 v_3 v'} V_{v'v_1 v v_4} + V_{v_1 v'v v_4} V_{v_2 v v_3 v'}] \right\}. \end{aligned} \quad (\text{S7})$$

Here l is a parameter running from 0 from $+\infty$, and $\dot{\Pi}$ represents derivatives $\Lambda \partial_\Lambda$ of the functions,

$$\begin{aligned} \Pi_{v'v''}^{\text{pp}}(\Lambda) &= \int \frac{dk}{2\pi} \frac{n_f(-\varepsilon_v(k)) - n_f(\varepsilon_{v'}(k))}{\varepsilon_v(k) + \varepsilon_{v'}(k)} [\Theta_{<}(\varepsilon_v(k)) \Theta_{<}(\varepsilon_{v'}(k))] \\ \Pi_{v'v''}^{\text{ph}}(\Lambda) &= \int \frac{dk}{2\pi} \frac{n_f(\varepsilon_v(k)) - n_f(\varepsilon_{v'}(k))}{\varepsilon_v(k) - \varepsilon_{v'}(k)} [\Theta_{<}(\varepsilon_v(k)) \Theta_{<}(\varepsilon_{v'}(k))] \end{aligned}$$

where $n_f(\varepsilon)$ is the Fermi-Dirac distribution function, and $\Theta_{<}(\varepsilon) = \frac{|\varepsilon|/[\Lambda]}{e^{|\varepsilon|/[\Lambda]} - 1}$, with $\Lambda = \Lambda_0 e^{-l}$, introduced to continuously integrate out high energy modes in the renormalization group flow. For the initial condition at $l = 0$, Λ_0 is set to be much larger than the bandwidth, and the four point functions are initialized as $V_{ssxx} = V_{ssyy} = V_{xxss} = V_{yyss} = J'$, $V_{xxsx} = V_{syyx} = V_{xxsx} = V_{syyx} = -2J$, $V_{xssx} = V_{ysss} = V_{xssx} = V_{ysss} = U - J$, with others initialized at 0 in absence of intra-band interaction. The generated intra-band interactions in the renormalization group flow are kept in our calculation.

S-3. CALCULATION OF SUSCEPTIBILITY

In presence of an external perturbation $\delta H = \int dz \sum_{v\alpha v'\alpha'} h_{v\alpha, v'\alpha'} \psi_{v\alpha}^\dagger \psi_{v'\alpha'}$, the susceptibility is obtained from linear response theory,

$$\begin{aligned} \chi_{v_1 \alpha_1, v_2 \alpha_2; v_3 \alpha_3, v_4 \alpha_4} &= \frac{\partial \langle \psi_{v_2 \alpha_2}^\dagger \psi_{v_3 \alpha_3} \rangle}{\partial h_{v_1 \alpha_1, v_4 \alpha_4}} \\ &= -\delta_{\sigma_1 \sigma_3} \delta_{\sigma_2 \sigma_4} \delta_{v_1 v_3} \delta_{v_2 v_4} \Pi_{v_1 v_2}^{\text{ph}}(\Lambda_0) \\ & \quad - \Gamma_{v_1 \sigma_1, v_2 \sigma_2; v_3 \sigma_3, v_4 \sigma_4} \Pi_{v_1 v_4}^{\text{ph}}(\Lambda_0) \Pi_{v_2 v_3}^{\text{ph}}(\Lambda_0) \end{aligned} \quad (\text{S8})$$

where the self-energy corrections are neglected following a standard approximation in simplification of functional renormalization group flow [30]. The first term in Eq. (S8) is the non-interacting part, and the specification to $v_1 = v_3 = s$ and $v_2 = v_4 = p_x$ (or p_y) leads to the expression of χ_{sp}^0 at the zero temperature limit. The susceptibilities in the channels of $\hat{\mathcal{B}}_{j_s, m_s, m_l; q}$ (Eq. (4)) have a block diagonal form,

$$\begin{aligned} \chi_{j_s, m_s, m_l}(q, q') &= \\ & \sum U_{j_s, m_s, m_l; q; v_4 \sigma_4, v_1 \sigma_1} U_{j_s, m_s, m_l; q'; v_2 \sigma_2, v_3 \sigma_3}^* \chi_{v_1 \sigma_1, v_2 \sigma_2; v_3 \sigma_3, v_4 \sigma_4} \end{aligned} \quad (\text{S9})$$

The symbol \sum performs summation over the indices $v_1 \sigma_1$, $v_2 \sigma_2$, $v_3 \sigma_3$, and $v_4 \sigma_4$. The unitary transformation is determined according to the definition of $\hat{\mathcal{B}}$ operators as,

$$U_{j_s, m_s, m_l; q; v\sigma, v'\sigma'} = (-)^{q+1} i^{2\sigma} C_{\frac{1}{2} \frac{1}{2}}(-\sigma, \sigma' | j_s m_s) T_{qv}^* T_{q+m_l, v'} \quad (\text{S10})$$

with T the matrix corresponds to transformation of s - and p -orbitals into the angular momentum basis (Eq. (4)). The susceptibility towards the order formation in \hat{O}_{m_s} channels is obtained as

$$\chi_{\text{SO}} = \chi_{1m_s, -1}(0, 0) - \chi_{1m_s, -1}(0, 1) = -\Pi_{sp}^{\text{ph}}(\Lambda_0) - [V_{xxsx}(l \rightarrow +\infty) - V_{xxsx}(l \rightarrow +\infty)] [\Pi_{sp}^{\text{ph}}(\Lambda_0)]^2. \quad (\text{S11})$$

The numerical results shown in the main text are obtained by solving the full flow equation. The analytic expression in Eq. (7) is obtained in the framework of renormalization group flow by solving the flow equation keeping the divergent ($\sim \Delta^{-1/2}$) contributions only, yielding $\partial_l V_{xxsx} = -\dot{\Pi}_{sp}^{\text{ph}} V_{xxsx}^2$.

S-4. FREE ENERGY OF THE SPIN-ORBIT INTERTWINED ORDER

Having a diverging correlation length in $\langle \hat{\mathcal{O}}_{m_s}^\dagger(z) \hat{\mathcal{O}}_{m_s}(z') \rangle$ implies the operator acquires an expectation value $\langle \hat{\mathcal{O}}_{m_s} \rangle = \Phi_{m_s}$, which is a three-component complex field. From SU(2) symmetry, the associated Ginzburg Landau free energy reads as

$$F = -r\Phi^\dagger\Phi + c_0(\Phi^\dagger\Phi)^2 + c_2(\Phi^\dagger\vec{L}\Phi) \cdot (\Phi^\dagger\vec{L}\Phi) + O(|\Phi|^6), \quad (\text{S12})$$

with L_x, L_y, L_z the standard spin-1 representation matrix of SU(2) group. To relate to our Fermionic theory, the phenomenological couplings r, c_0 and c_2 are calculated with a Hubbard-Stratonovich transformation as

$$\begin{aligned} r &= [J + J' - U] + \int \frac{dk}{2\pi} \frac{[J + J' - U]^2}{\varepsilon_p(k) - \varepsilon_s(k)}, \\ c_0 &= \frac{1}{2} \int \frac{dk}{2\pi} \frac{[J + J' - U]^4}{[\varepsilon_p(k) - \varepsilon_s(k)]^3}. \end{aligned} \quad (\text{S13})$$

In our theory, the coefficient c_2 vanishes for an accidental symmetry, causing an emergent SU(3) symmetry in the free energy. Then all states with the same order parameter amplitude $\sqrt{\Phi^\dagger\Phi}$ are degenerate in energy, although there are two distinctive states analogous to the polar and ferromagnetic phases in spin-1 superfluids [32, 33]. The order parameter strength is then given by $\sqrt{\frac{r}{2c_0}}$, and its small band gap limit is given in the main text.

However the above degeneracy is lifted by considering a circular motion induced Zeeman splitting for electrons, which is described by a Hamiltonian

$$\Delta H = \delta \int dz \left[i\hat{\Psi}_{x\uparrow}^\dagger \hat{\Psi}_{y\uparrow} - i\hat{\Psi}_{x\downarrow}^\dagger \hat{\Psi}_{y\downarrow} + H.c. \right]. \quad (\text{S14})$$

This leads to a symmetry-breaking term in the Free energy,

$$\Delta F = -\delta \sum_{m_s} m_s |\Phi_{m_s}|^2 \int \frac{dk}{2\pi} [\varepsilon_p(k) - \varepsilon_s(k)]^{-2}. \quad (\text{S15})$$

Minimizing the total free energy leads to $\Phi_+ = \phi, \Phi_0 = \Phi_- = 0$ for $\delta > 0$. The remaining unbroken $U(1)$ symmetry, $\phi \rightarrow \phi e^{i\theta}$, corresponds to the rotation symmetry around the z direction.

S-5. QUASI-PARTICLE HAMILTONIAN

Having an order $\Phi_+ = \phi, \Phi_0 = \Phi_- = 0$, the bare electrons turn into dressed quasi-particles, whose Hamiltonian reads as $H_{QP} = H_0 + H_{SOI}$, with

$$H_{SOI} = -(U - J - J') \int dz \left[\phi^* \hat{\mathcal{O}}_{+1}(z) + H.c. \right]. \quad (\text{S16})$$

Its explicit form in terms of $\hat{\Psi}$ operators is given in Eq. (8), where we have invoked spin-1/2 and spin-1 matrices

$$\sigma_+ = \begin{bmatrix} 0 & 2 \\ 0 & 0 \end{bmatrix}, L_- = \begin{bmatrix} 0 & 0 & 0 \\ 2 & 0 & 0 \\ 0 & 2 & 0 \end{bmatrix}. \quad (\text{S17})$$

The eigenmodes describing quasi-particles are introduced through a unitary transformation,

$$\begin{bmatrix} \tilde{\Psi}_{+\uparrow}(k) \\ \tilde{\Psi}_{0\downarrow}(k) \\ \tilde{\Psi}_{-\uparrow}(k) \end{bmatrix} = \begin{bmatrix} 1 & 0 & 0 \\ 0 & \cos(\vartheta_k/2)e^{i\varphi/2} & -\sin(\vartheta_k/2)e^{-i\varphi/2} \\ 0 & \sin(\vartheta_k/2)e^{i\varphi/2} & \cos(\vartheta_k/2)e^{-i\varphi/2} \end{bmatrix} \begin{bmatrix} \hat{\Psi}_{+\uparrow}(k) \\ \hat{\Psi}_{0\downarrow}(k) \\ \hat{\Psi}_{-\uparrow}(k) \end{bmatrix}, \quad (\text{S18})$$

$$\begin{bmatrix} \tilde{\Psi}_{+\downarrow}(k) \\ \tilde{\Psi}_{0\uparrow}(k) \\ \tilde{\Psi}_{-\downarrow}(k) \end{bmatrix} = \begin{bmatrix} \cos(\vartheta_k/2)e^{-i\varphi/2} & \sin(\vartheta_k/2)e^{i\varphi/2} & 0 \\ -\sin(\vartheta_k/2)e^{-i\varphi/2} & \cos(\vartheta_k/2)e^{i\varphi/2} & 0 \\ 0 & 0 & 1 \end{bmatrix} \begin{bmatrix} \Psi_{+\downarrow}(k) \\ \Psi_{0\uparrow}(k) \\ \Psi_{-\downarrow}(k) \end{bmatrix}, \quad (\text{S19})$$

with

$$\cos \vartheta_k = [\varepsilon_p(k) - \varepsilon_s(k)] / \sqrt{[\varepsilon_p(k) - \varepsilon_s(k)]^2 + 2(U - J - J')^2 |\phi|^2},$$

$$\sin \vartheta_k = (U - J - J') |\phi| / \sqrt{[\varepsilon_p(k) - \varepsilon_s(k)]^2 + 2(U - J - J')^2 |\phi|^2},$$

and $\varphi = \arg(-i\phi^*)$. We emphasize that the renormalized modes $\tilde{\Psi}_{m_l, \alpha}$ still mainly carry their original spin moment and angular momentum.

The induced quasi-particle Hamiltonian associated with the conduction band is then obtained to be

$$H_{\text{SOI}} = \int \frac{dk}{2\pi} \frac{\lambda_{\text{so}}(k)}{2} \left[\tilde{\Psi}_{+\uparrow}^\dagger(k) \tilde{\Psi}_{+\uparrow}(k) + \tilde{\Psi}_{-\downarrow}^\dagger(k) \tilde{\Psi}_{-\downarrow}(k) - \tilde{\Psi}_{-\uparrow}^\dagger(k) \tilde{\Psi}_{-\uparrow}(k) - \tilde{\Psi}_{+\downarrow}^\dagger(k) \tilde{\Psi}_{+\downarrow}(k) \right], \quad (\text{S20})$$

with a momentum dependent SOI strength

$$\lambda_{\text{so}}(k_z) = [\varepsilon_p(k_z) - \varepsilon_s(k_z)] / 2 - \sqrt{[\varepsilon_s(k_z) - \varepsilon_p(k_z)]^2 / 4 + (J - U - J')^2 |\phi|^2 / 2}.$$

Near the band edge, the induced SOI strength further simplifies to the expression given in Eq. (1)

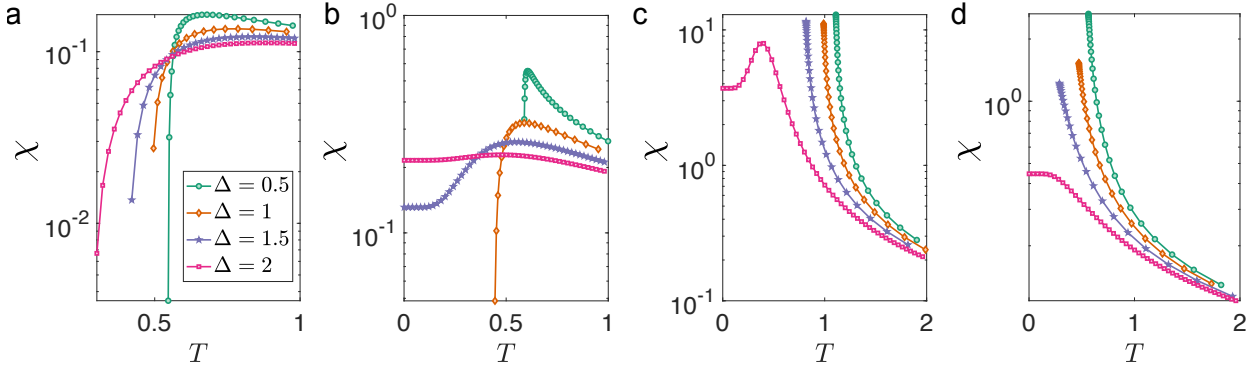


FIG. S1. **The susceptibility corresponding to the channel of $[\mathcal{B}_{0,0,1;0} - \mathcal{B}_{0,0,1;-1}] / \sqrt{2}$ with renormalization group calculation.** The plots correspond to different choices of interaction strengths (U, J, J') and band gap (Δ) in the tight binding model. The tunneling of the s -orbital electron, or one half of bandwidth of the s -band is set as the energy unit here. In (a, b, c, d), we have $(U, J, J') = (2, -1, -0.5)$, $(2, 0.1, -0.5)$, $(2, 1, -0.5)$, and $(2, -1, 0.5)$, respectively. This susceptibility remains non-divergent at low temperature in a, and b. In c, and d, we find a divergent susceptibility, which causes the strong suppression of spin-orbit intertwined order at low temperature.

S-6. SYMMETRY PROPERTIES

In this supplementary section, we provide more details of our symmetry analysis. In the basis of $\hat{\Psi}_{q\alpha}$, the anti-unitary time-reversal symmetry transformation (\mathcal{T}) is represented as [34],

$$\mathcal{T} \hat{\Psi}_{q\alpha} \mathcal{T}^{-1} = i^{-2\alpha} (-1)^q \hat{\Psi}_{-q, -\alpha}, \quad (\text{S21})$$

$$\mathcal{T} \hat{\Psi}_{q\alpha}^\dagger \mathcal{T}^{-1} = i^{2\alpha} (-1)^q \hat{\Psi}_{-q, -\alpha}^\dagger. \quad (\text{S22})$$

$$(\text{S23})$$

The spatial parity transformation (\mathcal{P}) is represented as

$$\mathcal{P}\hat{\Psi}_{q\alpha}\mathcal{P}^\dagger = (-1)^q\hat{\Psi}_{q,\alpha}. \quad (\text{S24})$$

Under spatial rotation (R_θ) around the z -axis, we have

$$R_\theta\hat{\Psi}_{q\alpha}R_\theta^\dagger = \hat{\Psi}_qe^{iq\theta} \quad (\text{S25})$$

Then the corresponding symmetry properties of the composite operators $\mathcal{B}_{j_s, m_s, m_l; q}$ are derived as listed in Table I in the main text.

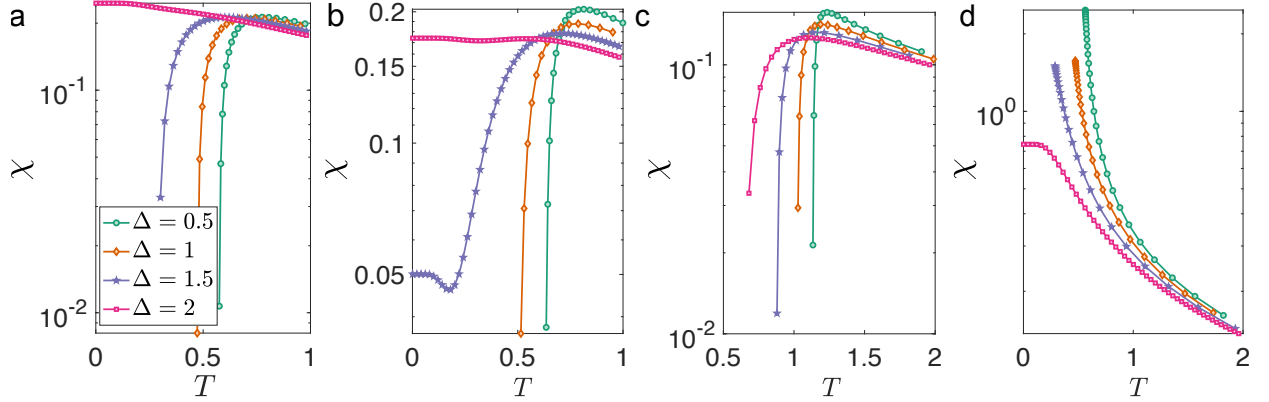


FIG. S2. **The susceptibility corresponding to the channel of $[\mathcal{B}_{1, m_s, -1; 0} + \mathcal{B}_{1, m_s, -1; 1}]/\sqrt{2}$.** The parameter choices are the same as in Fig. S1. This susceptibility remains non-divergent at low temperature in **a**, **b** and **c**. In **d**, we find the susceptibility diverges.

S-7. SUSCEPTIBILITIES IN OTHER CHANNELS

In this supplementary section, we provide other relevant susceptibility channels which affect the spin-orbit intertwined order in the functional renormalization group flow. In Fig. S1, we provide the susceptibility corresponding to a time-reversal odd spin singlet channel,

$$[\mathcal{B}_{0, 0, 1; 0} - \mathcal{B}_{0, 0, 1; -1}]/\sqrt{2}. \quad (\text{S26})$$

In Fig. S1(a, b), this susceptibility does not diverge at low temperature, which then does not cause suppression of the spin-orbit intertwined order as shown in Fig. 2(a, b) in the main text. In Fig. S1(c, d), the susceptibility diverges at low temperature, which causes the strong suppression of the spin-orbit intertwined order as shown in Fig. 2(c, d).

In Fig. S2, we provide the susceptibility corresponding to a time-reversal odd spin triplet channel,

$$[\mathcal{B}_{1, m_s, -1; 0} + \mathcal{B}_{1, m_s, -1; 1}]/\sqrt{2}. \quad (\text{S27})$$

This susceptibility is non-divergent in Fig. S2(a, b, c). In Fig. S2(d), this susceptibility diverges.

S-8. ESTIMATE OF INTERACTION STRENGTHS

Taking the *ab initio* band structure of a right-banded peptide helix [29], the low-energy properties of the molecule are captured by a three-orbital model having p_x , p_y , and p_z orbitals—the p_z orbital here is analogous to the s -orbital

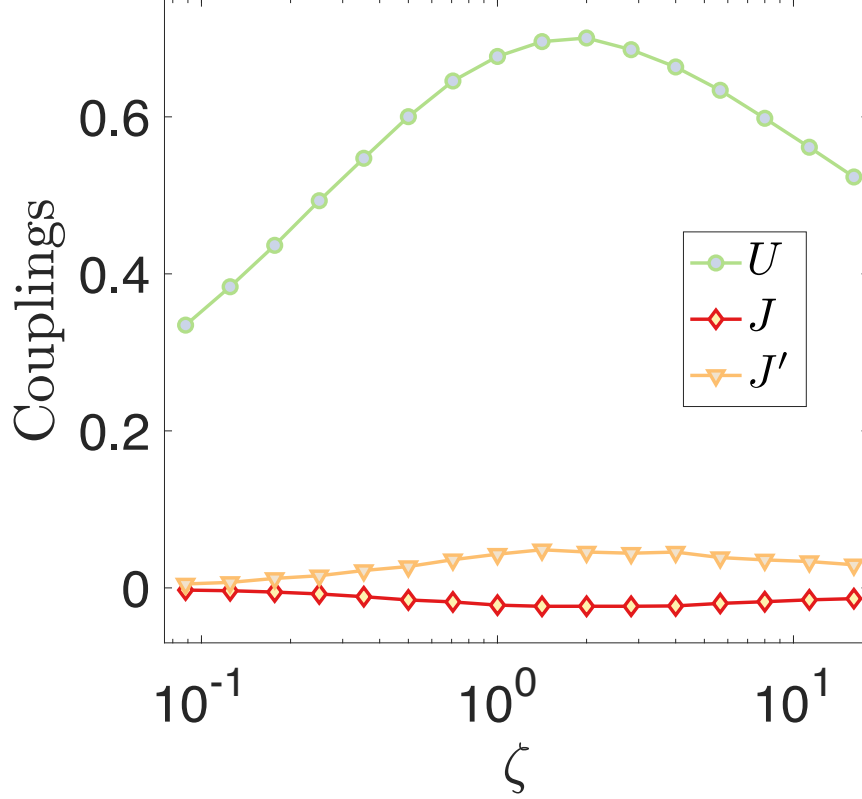


FIG. S3. **The interaction strengths in the tight-binding model.** The energy unit in this plot is $E_0 \equiv \frac{e^2}{\sqrt{a_{\perp}a_{\parallel}}}$, and the varied parameter ζ is a ratio a_{\parallel}/a_{\perp} (see the description in Sec. S-8.)

in our theory as they obey the same rotation symmetry. We estimate the interaction strength by taking a harmonic approximation to the Wannier functions of these orbitals ($\phi_{x,y,z}(\vec{r})$ [35],

$$\phi_{x,y,z}(\vec{r}) \propto r_{x,y,z} \exp \left\{ -\frac{1}{2} \sqrt{\left(\frac{r_x}{a_{\perp}}\right)^2 + \left(\frac{r_y}{a_{\perp}}\right)^2 + \left(\frac{r_z}{a_{\parallel}}\right)^2} \right\}, \quad (\text{S28})$$

where r_x, r_y, r_z are the three spatial coordinates, a_{\perp} corresponds to radius of the molecule in the transverse direction, and a_{\parallel} one-half of the size of the repetition unit along the molecular elongation direction. The bare interaction strengths at the starting point of the renormalization group flow are estimated by projecting the Coulomb interaction to the three p -orbitals, from which we have

$$V_{v_1, v_2, v_3, v_4}/2 = \int d^3\vec{r} d^3\vec{r}' \phi_{v_1}^*(\vec{r}) \phi_{v_4}(\vec{r}) \frac{e^2}{|\vec{r}-\vec{r}'|} \phi_{v_2}^*(\vec{r}') \phi_{v_3}(\vec{r}'), \quad (\text{S29})$$

with $\frac{e^2}{|\vec{r}-\vec{r}'|}$ the Coulomb interaction between two electrons. The interaction strengths $U, J,$ and J' in Eqs. (S2,S3,S4) are obtained from $U = V_{xzzx} + V_{zxzx}/2$, $J = -V_{zxzx}/2$, and $J' = V_{zzxx}$. In this calculation, the interaction strengths are determined by $E_0 \equiv \frac{e^2}{\sqrt{a_{\perp}a_{\parallel}}}$, and the ratio $\zeta \equiv a_{\parallel}/a_{\perp}$. The results are shown in Fig. S3, where E_0 is set as an interaction energy unit. With a choice of $\sqrt{a_{\perp}a_{\parallel}} = 0.5\text{nm}$, E_0 is about 5eV. For a wide range choice of the ratio ζ , U is about 1.5 ~ 3.3eV, and both J and J' are below 0.1eV, an order of magnitude smaller than U .